Preprint Cambridge Centre for Computational Chemical Engineering ISSN 1473 – 4273

Sooting tendency and particle size distributions of n-heptane/toluene mixtures burned in a wick-fed diffusion flame

Maria Botero [1], Sebastian Mosbach [1], Markus Kraft [1,2]

released:

[1] Department of Chemical Engineering and Biotechnology
University of Cambridge
New Museums Site
Pembroke Street
Cambridge, CB2 3RA
United Kingdom
E-mail: mk306@cam.ac.uk

[2] School of Chemical and Biomedical Engineering
Nanyang Technological University
62 Nanyang Drive
637459
Singapore

Preprint No. 153

Keywords: soot, surrogate fuel, smoke point, particle size distribution, particle morphology

Edited by
Computational Modelling Group
Department of Chemical Engineering and Biotechnology
University of Cambridge
New Museums Site
Pembroke Street
Cambridge CB2 3RA
United Kingdom

Fax: + 44 (0)1223 334796
E-Mail: c4e@cam.ac.uk
World Wide Web: http://como.cheng.cam.ac.uk/

Abstract

The sooting characteristics of binary mixtures of n-heptane and toluene and a commercial gasoline were studied. The experiment involves the non-premixed combustion of the fuel in wick-fed burner. The particle size distributions (PSDs) of soot were measured at the tip of flames of different heights, using a differential mobility spectrometer (DMS). Transmission electron microscopy (TEM) was used to investigate the morphology of the particles formed. Pure n-heptane and toluene were studied along with blends of 10%, 30%, and 50% by volume of toluene in n-heptane. The addition of toluene to heptane shifts the PSD to larger diameters. As toluene is added to n-heptane the dependence of soot particle size on flame height changes from resembling a paraffinic to resembling an aromatic fuel in a non-linear fashion. A tolerance to toluene addition at the lowest flow rates was found, where particles were not detected. A commercial gasoline with approximately 44% by mass of aromatics was also analysed. The smoke point (SP) and PSDs are similar to the mixture 50% toluene 50% n-heptane, but the mean aggregate mobility size, number of particles and primary particle size formed by the gasoline are smaller.

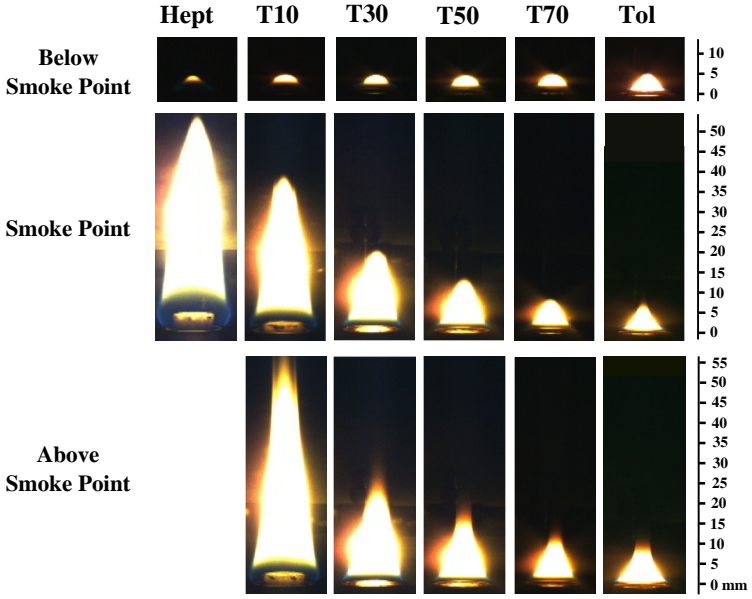

Images of studied flames at different sooting stages. Toluene concentration increases from left to right. Top row flames are below the smoke point and have a height of 5 mm. Middle row flames are at the smoke point, and bottom row flames are above the smoke point.

1 Introduction

Commercial transportation fuels such as gasoline are mixtures of hundreds of hydrocarbons. The primary chemical classes of hydrocarbons in fuels are paraffins, olefins and aromatics. Although the composition of these fuels are variable, there are some common trends [10, 19, 47]. The high complexity of fuels encouraged the search for mixtures of limited components to ease the development of new combustion technologies through computational tools, and to generate insight and understanding of underlying fundamental processes.

A surrogate fuel is defined as a mixture of a small number of hydrocarbons which aims to emulate chemical and physical properties of a real fuel. The study of surrogate fuels and its formulation has been used basically for the development of kinetic mechanisms that describe the real kinetic behaviour of non-sooting phenomena [16, 42, 55]. Most of these studies on surrogate fuels are focused on the ignition delay time, autoignition and extinction characteristics. However, the knowledge regarding the soot formation process from single as well as mixtures of hydrocarbons remains in a poor stage [34].

In the last century strong efforts were made to understand the mechanisms of soot formation [23, 57]. There is now an agreement that the pathway begins with the formation of molecular precursors such as polyacetylenes and polycyclic aromatic hydrocarbons (PAHs) [21]. The rate limiting reaction is the formation of the first aromatic ring, for which various mechanisms have been proposed [2, 62, 63]. Collision and sticking of PAHs conducts to particle inception [20, 39, 49]. Once primary particles are formed, these nascent soot particles undergo surface growth [48] (and in some systems competing oxidation reactions), and the small particles will agglomerate into larger fractal structures [20, 41, 43, 46]. However, there are still many unresolved questions in this process, some of them are the transition between gas and solid phase (particle inception), the growth of such particles and the influence of the fuel composition in the entire process [36]. In the last decade efforts have been focused on experimentally understand such processes [1, 38, 40, 54] as well as to model and predict them [8, 20, 43, 50, 59, 61].

Significant contribution analysing the smoking process of some hydrocarbons and their mixtures have been made recently [17, 34], showing that the soot formation have a strong correlation with hydrocarbons' structure. Some studies on the sooting tendency of surrogate fuels and surrogate mixtures have appeared [9, 17, 18, 56, 60, 66]. One of the targets used to assess a fuel surrogate mixture in terms of its sooting propensity is the threshold sooting index (TSI) [7, 45] that is based on the smoke point (SP) [3]. This property enables the analysis of hydrocarbon mixtures because of its linear relationship to fuel composition [22, 37], facilitating its estimation over a large amount of possible surrogate mixtures [15]. However, no information on the characteristics of the soot particles is available through this targeted property, and experimental data on this matter remains scarce.

The aromatic content has been considered to be responsible for the formation of soot particles [4, 29, 30]. In an optically accessible combustion chamber study, it was found that the aromatic content dominates over effects of partial premixing and results in higher total soot mass [29, 30]. An opposite trend was found by *Wang et al* [64] on experiments

and simulation of a diesel engine. A higher toluene content in n-heptane/toluene mixtures actually produced the lowest soot emissions, due to the slightly longer ignition delay, indicating that the mixing process also plays an important role. Binary mixtures of n-heptane/iso-octane, n-heptane/toluene and iso-octane/toluene have been investigated in counterflow diffusion flames [9]. Results showed a tolerance in the mixing of toluene below which its effect on soot formation was minimal. The tolerance to toluene addition has been observed also in shock tube experiments [26].

The simplest and most studied surrogate in diesel engines is the mixture of n-heptane and toluene [13, 27, 33, 64, 66]. Higher concentrations of toluene in the mixture results in a longer ignition delay [13, 27]. In an optical combustion chamber, experiments showed that the higher the toluene content the more premixed combustion occurs. As a small quantity of toluene (5%) was added to n-heptane, the soot mass concentration increased while generally keeping the same diameter [13]. However, when the toluene content was increased to 10% both mass concentration and particle size increased, resembling that produce from diesel fuel. A similar observation was also made in a co-flow diffusion flame [66], where the aromatic addition seemed to contribute to the soot volume fraction by increasing soot aggregate concentrations but having insignificant effect on the soot morphology.

Even though important steps have been taken towards the understanding of soot formation in commercial fuels through the experimentation with surrogate fuels, scarcity of detail information remains, particularly on the soot particle size distributions. The purpose of this paper is study soot particles formed from fuel mixtures to learn more about the nature of soot as well as providing additional information that can aid modelling, such as the interpretation of the mobility diameter and the fractal structure of soot and its degree of sintering.

The soot PSDs and morphology in the non-premixed combustion of n-heptane and toluene mixtures was investigated. In order to capture the influence of aromatic addition, we characterise the soot particles formed in a wick-fed laminar diffusion flame of pure n-heptane, toluene and its mixtures at different flame heights, using differential mobility spectroscopy (DMS). In-flame soot samples were analysed by transmission electron microscopy (TEM). A commercial petrol-station gasoline was studied as well in order to compare its sooting behaviour with the surrogate mixtures.

2 Experimental methodology

2.1 Soot particle size measurements

The fuels tested are: n-heptane, toluene, and their mixtures with volumetric additions toluene of 10% (H90T10), 30% (H70T30) and 50% (H50T50). A commercial unleaded gasoline (RON 95) was also tested, GC-MS was used to obtain the fuel composition.

The experimental set-up and procedure used in this study is the same as described previously in [5, 6]. A standard smoke point lamp where the fuel is supplied via a wick was used to generate a laminar diffusion flame [3]. The flame height was adjusted by increas-

ing the wick exposure (*i.e.* increasing the fuel flow rate). At each flame height the fuel flow rate was calculated from the weight loss of the burner as described by [65].

Figure 1 depicts the flame sampling system, detailed information can fe found in [6]. The soot particles were sampled using a stainless steel probe with 8 mm inner diameter, enclosed by two water cooling jackets either side of a 0.3 mm sampling hole. The sample is drawn into a constant nitrogen dilution flow of approximately 8 litres/min at 0.25 bara. A secondary diluter within the particle analyser reduces the load to the particle classifier. The dilution in this experiments is calculated to be in the range 10000-15000. The residence time of the gas sample passing through the orifice is less than 8 μs before it was diluted with cold nitrogen. At these experimental conditions independence of the PSD with dilution ratio was achieved [5, 6].

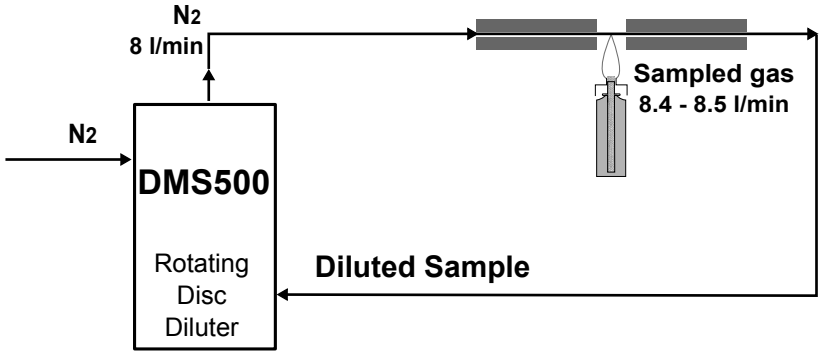

Figure 1: *Sampling system for particle size analysis.*

The particle analyser used in the present work is a Differential Mobility Spectrometer 500 (DMS) developed and manufactured by Cambustion Ltd. The particles are sized based on their mobility diameter, which is the diameter of a sphere with the same migration velocity as the particle of interest in a constant electric field.

The soot particles are always sampled at the tip of the flame, and therefore at the centerline, for a series of different flame heights. The flame height was adjusted and sampled again at the tip, this is repeated until the tip of the flame is no longer defined for sampling. Each flame height is sampled for 30 seconds, which corresponds to at least 6 averaged PSDs measured by the DMS. This procedure is repeated at least three times for each fuel.

2.2 Temperature measurements

Centerline temperature measurements were performed with an uncoated 75 μm type R thermocouple (Pt/Pt-13%R), using a rapid insertion procedure to minimise soot deposition [35]. The constant-tension thermocouple design [12] was used as a reference for the set-up. Detailed information on the measurements and correction due to thermocouple radiation losses can be found elsewhere [6]. Radiation correction was in the range of 15-50 K.

2.3 Thermophoretic sampling and HRTEM

The technique used is a common in-flame sampling method for microscopy imaging is based on the phenomenon of thermophoresis occurring in the vicinity of a cold probe introduced inside the flame. Soot particles are driven thermophoretically to the cold wall of the probe and are ultimately captured on its surface [14]. A fast insertion technique is used to protect the grid from thermal damage. A pneumatic solenoid was use to drive the sample in and out the flame in a very short period. The system was calibrated with a fast speed camera. Ten seconds were allowed between insertions to let the grid cool down.

Holey carbon films on 300 mesh cooper grids were used to collect soot particles. TEM images were taken using a JEOL 3011 microscope with an operating voltage of the microscope is 300 keV using a Lab6 filament. Gatan image software v3.4 was used for microscope operation. At least 10 images acquired in different regions of the grid (5-10 squares surrounding the grid centre) were selected for image analysis. The average primary particle size was determined using TEM images obtained under 15,000x and 40,000x magnifications, by measuring the diameter of more than 200 particles for each sample, using the image processing and analysis software ImageJ®. The data was fitted to lognormal distribution, and average primary particle size was extracted from raw data.

3 Results

The SP is defined as the '*maximum height (mm) of a smokeless flame of fuel burned in a wick-fed lamp*' [3]. It was measured for all fuels, heptane's SP could not be measured on this apparatus because it exceeded the maximum range of the smoke point lamp. TSI values based on the SP were calculated [22, 52, 65], methylcyclohexane was used as lower-bound with a TSI value of 5 and 1-methylnaphthalene as higher-bound with a value of 100.

Some of the sampled flames are presented in **Figure 2**. Starting from very short flames ($\sim$3 mm), and passing through the smoke point, the flow rate is increased until the tip of the flame is no longer defined, but a trail of soot emerges from the top of the flame. Given that the sampling point is always the tip of the flame, the largest flame tip that could be sampled for each fuel was considerably different. **Table 1** presents the smoke point and TSI of the studied fuels. Heptane has the largest smoke point, the highest flame sampled for heptane is 73 mm. Instead, toluene has the lowest smoke point ($\sim$7.8 mm), hence flame heights a few millimiters larger will have an undefined tip and a soot trail. For this reason the highest flame height sampled for toluene is $\sim$12 mm. As toluene is added to heptane the smoke point of the fuel mixture decreases indicating a larger sooting tendency, and according to our experimental procedure smaller flame heights were able to be sampled. This tendency is in agreement with previous studies [22, 65].

Table 2 presents the composition of gasoline fuel from GC-MS results. The aromatic content is approximately 44% by mass, with a significant amount of toluene ($\sim$ 14%), xylenes ($\sim$ 15.3%), trimethylbenzenes ($\sim$ 8.4%) and ethylbenzene ($\sim$ 3.7%) and smaller quantities of larger alkyl-benzenes. Saturated hydrocarbons have also a high content in the gasoline, $\sim$ 45%. Within this class of hydrocarbons, branched paraffins are predominant,

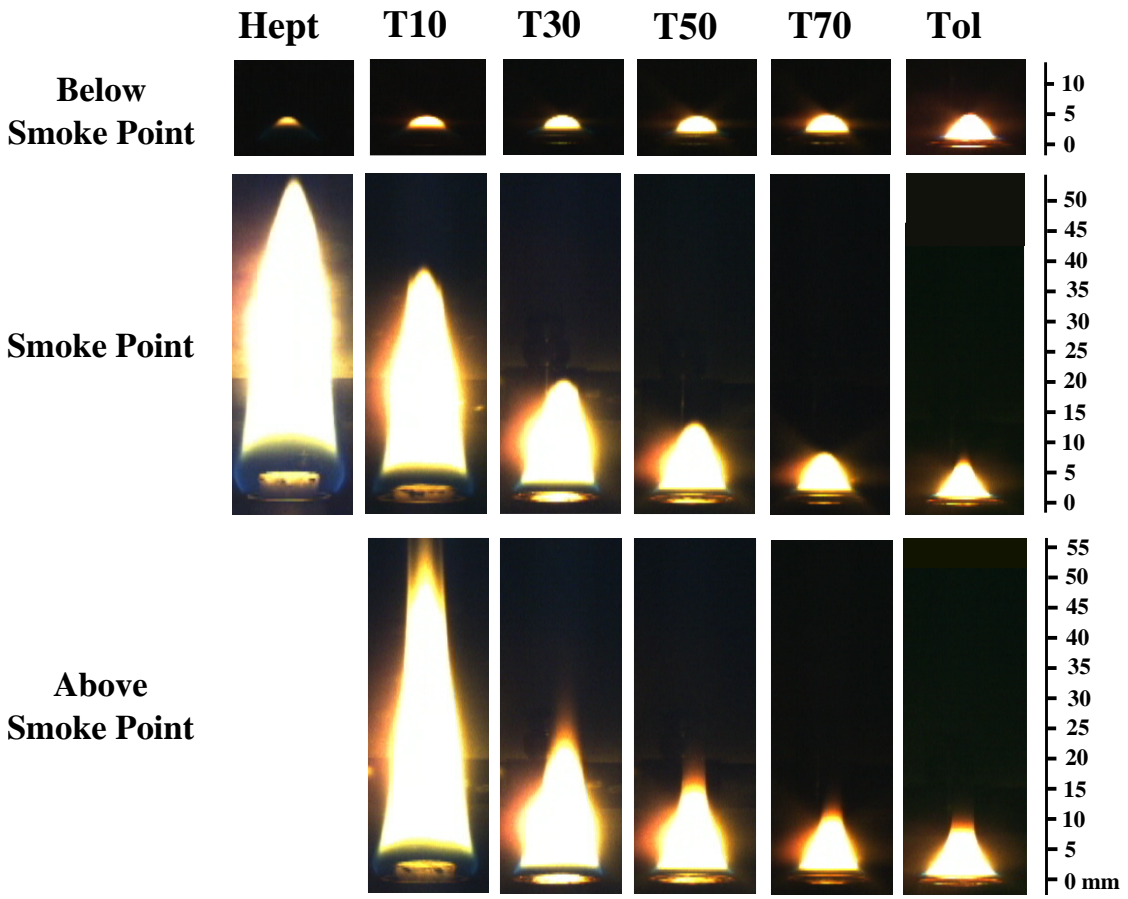

Figure 2: *Images of studied flames at different sooting stages. Toluene concentration increases from left to right. Top row flames are below the smoke point and have a height of 5 mm. Middle row flames are at the smoke point, and bottom row flames are above the smoke point.*

Table 1: *Smoke points of studied fuels.*

	Smoke point (mm)	TSI
Heptane	73.0 ± 18 *	-2.6
H90T10	39.0 ± 2.8	2.1 ± 3.30
H70T30	20.5 ± 1.7	11.0 ± 4.81
H50T50	12.0 ± 1.1	19.9 ± 6.53
H30T70	9.8 ± 0.8	30.5 ± 8.55
Toluene	7.8 ± 0.5	39.4 ± 10.1
Gasoline	11.8 ± 0.4	

*This value was reported by [65]. Values higher than 100 mm have been reported [7, 28, 45].

with small amounts of straight and cyclic paraffins. The tested gasoline presents a smoke point very similar to that of H50T50. This seems to be consistent with its aromatic content.

Table 2: *Chemical composition of studied gasoline.*

Fuel type	% mass
Aromatics	43.8
toluene	*14*
alkyl-benzenes	*29.7*
naphthalenes	*0.14*
Paraffins	44.7
straight	*6.6*
branched	*35.6*
cyclic	*2.5*
Olefins	11
Other	0.47

3.1 Temperature at the flame tip

The weight loss of the burner containing the liquid fuel was recorded to obtain a continuous measure of the fuel consumption at each flame height. The gradient of the least-squares regression line was used to determine the average fuel uptake rate. Excellent linearity was obtained, giving evidence of a constant flow rate at a given flame height. This result is consistent with a previous investigation [65].

Figure 3a shows the temperature at the sampling point (tip of the luminous flame) as a function of the fuel flow rate. It can be seen that as toluene is added to n-heptane the flow rates sampled were lower, as explained before. As the flow rate (*i.e.* flame height) increases, the temperature at the tip decreases. As the flow rate is increased the yellow luminosity in the flame also increases but the true stoichiometric flame lies below the observable luminous flame [25, 53]. The ratio of the luminous flame height to the true diffusion flame height increases as the flow rate is increased [25]. Therefore, the soot particles that are not completely oxidised at the stoichiometric flame would survive beyond. In this region between the diffusion flame and the luminous flame there is a high temperature oxidising environment where the soot particles would continue emitting greybody radiation until they are completely oxidised. In addition soot formation is larger as the flowrate is increased, resulting in higher losses through radiation. These may explain why the temperature at the tip of the luminous flame decreases as flow rate is increased.

The rate at which the tip temperature decreases is larger for toluene. For the same flow rate n-heptane exhibits the largest flame tip temperature, and as toluene is added the temperature decreases with pure toluene presenting the smallest temperatures. The calculated adiabatic flame temperature of toluene (2317 K) is larger than heptane's (2265 K) [24]. For this reason we speculate that lower temperatures observed as toluene concentration increases are due to stronger losses through soot radiation due to its larger sooting tendency, as shown in **Table 1** and discussed throughout the document. Gasoline exhibits flame tip temperatures similar to H50T50.

It is important to note that when comparing fuels at the same flow rate (hence similar flame heights) we are approximately comparing particles with the same residence time. However, at the same flow rate some fuels can be below the smoke point, while others can

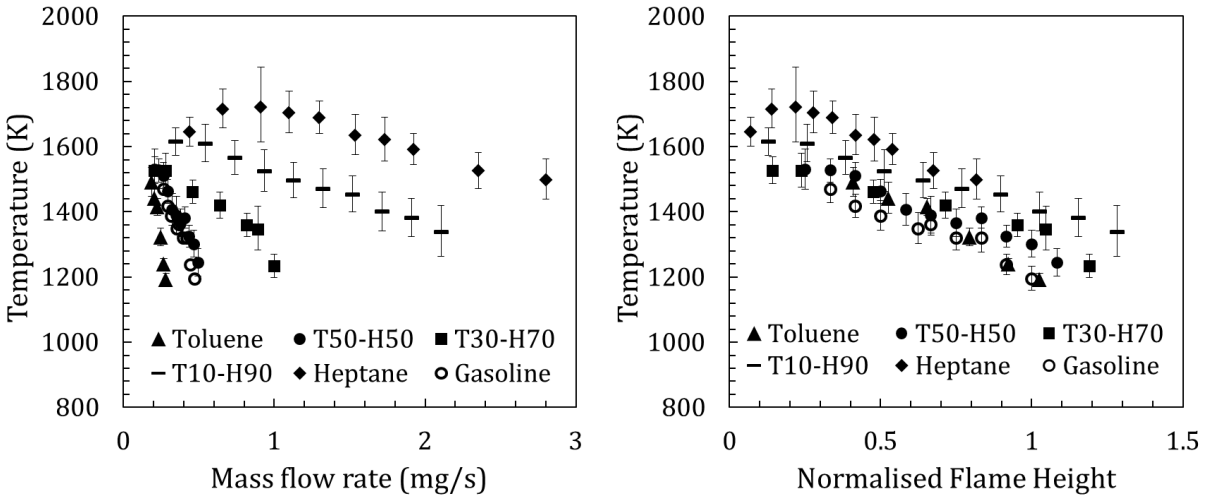

(a) *Tip of flame temperature vs. fuel flow rate*

(b) *Tip of flame temperature vs. flame height normalised by the smoke point*

Figure 3: *Temperature at the tip of different flames for all studied fuels. As flow rate and toluene concentration increases the temperature at the flame tip decreases. At the same sooting stage (normalised flame height) the fuels have similar flame tip temperature.*

be already emitting soot particles. For example at 10 mm flame height toluene is emitting particles, whilst H50T50 mixture is in a transition stage, but H70T30 and H90T10 are still below its smoke point. In order to investigate in greater detail the trends below and above the smoke point the normalised flame height is introduced. For each fuel the flame height is normalised by its smoke point. Values of normalised flame height below unity correspond to flames below the smoke point. Values greater than unity correspond to a smoking flame.

Figure 3b presents temperature as a function of normalised flame height. It can be seen now how most of the fuels have similar temperature at the same "sooting stage", with heptane showing the largest temperatures specially at very short flames. Below the smoke point (value of unity), toluene and all mixtures have nearly the same tip temperature considering the error bars, but H90T10 seems to have consistently higher values (approximately 100 K) and lying in-between n-heptane and the other mixtures. Above the smoke point, it appears that the sootier the fuel the smaller the tip temperature, this seems consistent with possible larger losses due to soot radiation.

3.2 Number density and mean mobility diameter of soot particles

From the PSD important parameters are calculated: the aggregate number density N (area under the curve) and the mean aggregate mobility diameter $\langle dp \rangle$. Most of the particles measured in these flames correspond to non-spherical aggregates and the measured mobility diameter assumes particle sphericity and neglects the effect of a rough surface and non-homogeneous charge. This should be accounted for in the interpretation of the mo-

bility diameter, given that the aggregate structure can lead to an increase in the particle surface area, therefore it is a measurement of the fractal aggregate mobility [58].

Figure 4 presents the calculated N and $\langle dp \rangle$ as a function of flame height for each fuel. At low flow rates N is large (**Figure 4a**) and $\langle dp \rangle$ is small (**Figure 4b**) suggesting the nucleation of primary particles. High number densities of young soot particles causes intense coagulation and result in a sharp decrease of N and larger particle sizes [51]. As the flow rate increases N stops decreasing and achieves a minimum and then remains relatively constant for heptane, but as toluene is added N tends to increase again.

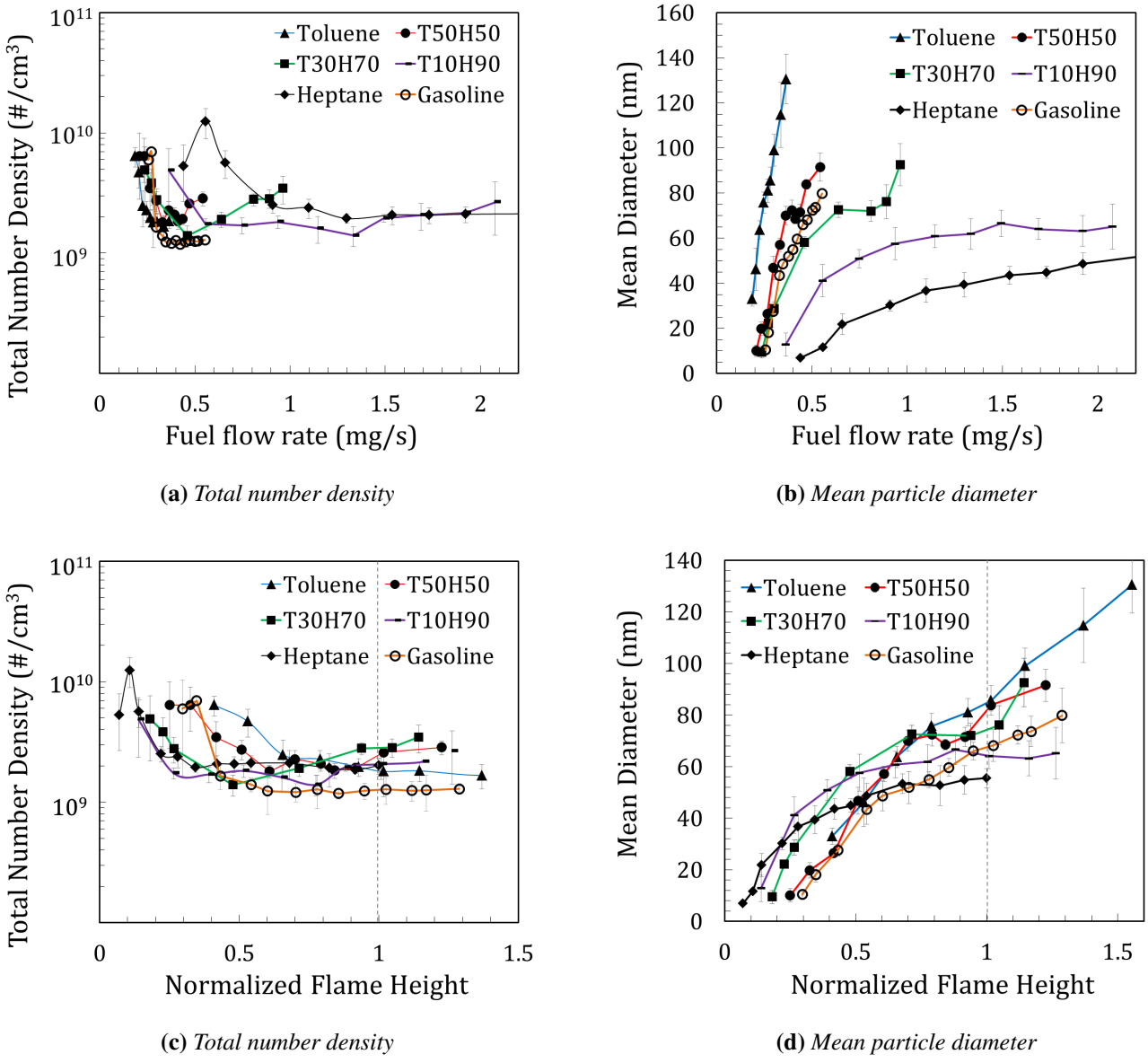

(a) *Total number density*

(b) *Mean particle diameter*

(c) *Total number density*

(d) *Mean particle diameter*

Figure 4: *Mean soot particle diameter and number of particles as a function of fuel flow rate and flame height normalised by the smoke point.*

Two different trends in $\langle dp \rangle$ growth are observed. Heptane follows the paraffin trend,

where as flow rate is increased $\langle dp \rangle$ achieves a maximum value and then remains constant [5]. H90T10 follow this trend but the particle sizes are larger. On the other hand toluene exhibits a continuous $\langle dp \rangle$ growth as flow rate is increased. H70T30 shows a transition between the two trends, as flow rate increases $\langle dp \rangle$ grows, but at some point it achieves a constant value, and with further flow rate increments $\langle dp \rangle$ resumes its growth. H50T50 exhibits a small $\langle dp \rangle$ growth pause period, with almost continuous particle growth throughout all the tested flow rates.

In general, heptane produces the smallest particles, and as toluene is added the soot particle size increases. The largest particle sizes are produced by pure toluene. Gasoline results lie between H70T30 and H50T50.

To compare again the evolution of N and $\langle dp \rangle$ at similar sooting stages between the fuels, plots against normalised flame height (as defined previously in **section 3.1**) are presented in **Figure 4**. The smoke point (value of unity in the plots) is denoted by a vertical dashed line. To the left of the smoke point line the sampled flames have a closed and defined tip and are not emitting soot, to the right of the line the flames are emitting soot and the tip is blurry but still defined without a soot trail.

In **Figure 4c** it can be seen that below the smoke point heptane, H90T10 and H70T30 have similar N values, while H50T50, toluene and gasoline exhibit higher values. As N decreases due to fast coagulation it achieves similar values for all the fuels.

The evolution of $\langle dp \rangle$ is depicted in **Figure 4d**. Below the smoke point heptane, H90T10 and H70T30 have similar $\langle dp \rangle$ and larger than H50T50, toluene and gasoline; here it is worth mentioning that their flame heights are larger and therefore the particles' residence time. As the flames approach the smoke point height $\langle dp \rangle$ intends to achieve a constant value, but only heptane and H90T10 effectively do. Heptane presents the smallest $\langle dp \rangle$ followed by H90T10 which is very close to all other fuels considering the experimental error. Close to and above the smoke point height the $\langle dp \rangle$ at the tip of H70T30, H50T50 and toluene's flames continue growing again with values relatively close.

Gasoline shows a continuous $\langle dp \rangle$ growth resembling an aromatic fuel. Particularly at initial sooting stages the particles sizes are similar to H50T50. As the gasoline flame approaches the smoke point, the $\langle dp \rangle$ at the flame tip reach smaller values than H50T50 and even H70T30.

3.3 Particle size distributions

The particle size distributions as a function of flame height for the pure fuels and their mixtures is presented in **Figure 5**. In grey are displayed the PSDs of the tip of flames below the smoke point, in solid black the PSD close to the smoke point, and black dashed above the smoke point. Toluene and heptane represent the higher and lower sooting boundaries respectively.

At a very small FH of 3 mm toluene shows a bi-modal PSD with a larger accumulation mode. At this flame height or one millimetre higher (4 mm) the PSD of the three mixtures consist of single mode of small particles, presumably primary particles in the nucleation stage (nucleation mode). As the volume of toluene in the mixture decreases so does the

width of the nucleation mode. The transition from a single mode PSD to a bimodal PSD occurs very quickly, in a matter of a few millimetres. It can be seen in the H50T50 and H70T30 mixtures that between 4 to 6 mm flame heights the PSD changes and a second mode of larger particles appears. This is due to an intense coagulation process caused by the large number and reactivity of young soot particles.

At flame heights of approximately 10 mm all the fuels exhibit a bimodal PSD with a larger accumulation mode, except for heptane that still forms a large nucleation mode. Close to the smoke point a similarity can be observed between the shape of the PSDs of toluene, H50T50 and H70T30 with a predominant mode of large particles. H90T10 and pure heptane present a PSD with multi-modal behaviour composed of a larger accumulation mode but significant modes of smaller particles. After the smoke point the PSDs at the tip of the flame consist on the enlargement of the accumulation mode.

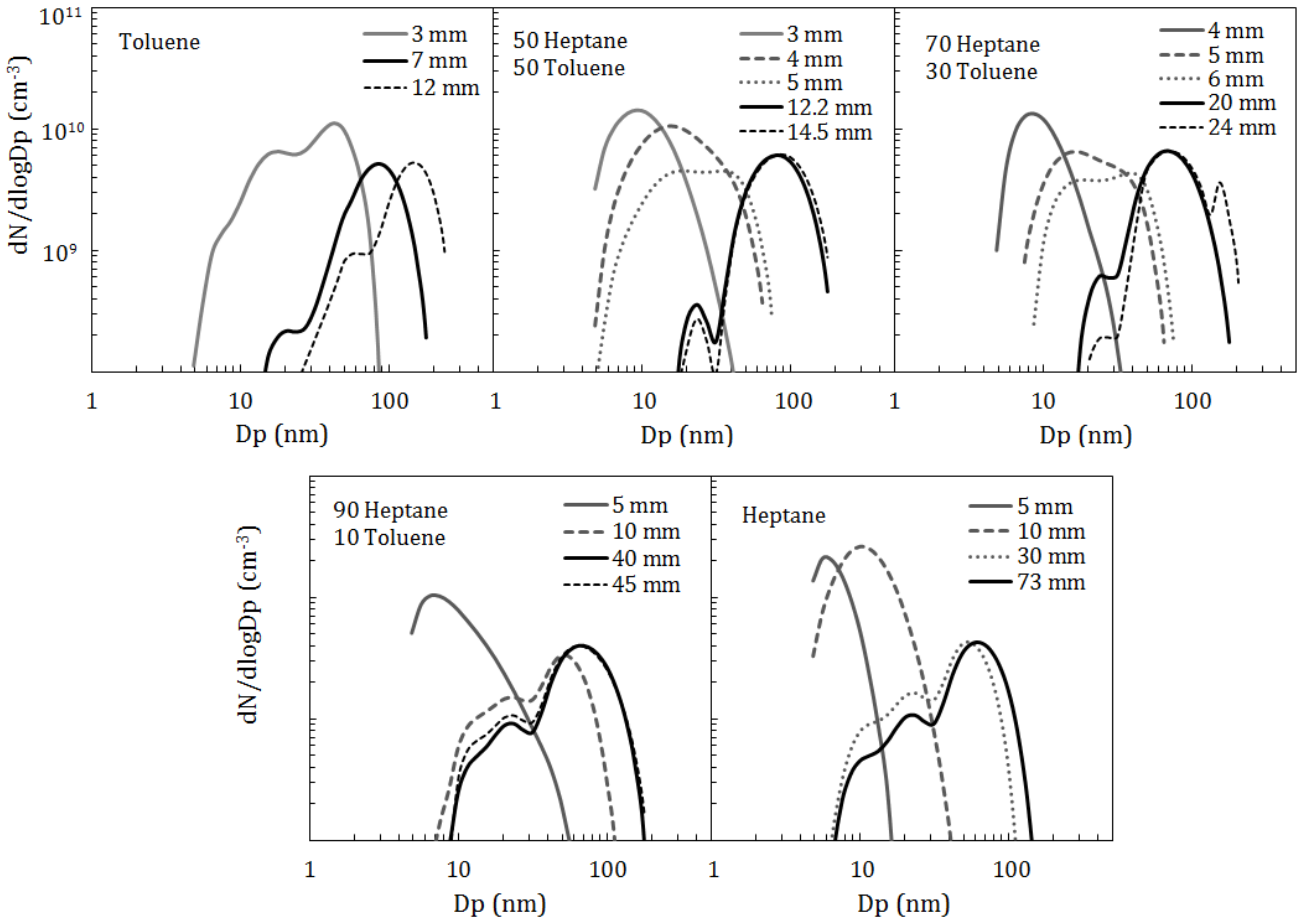

Figure 5: *Evolution of PSD at the tip of flames with different height for all tested fuels. Curves in grey correspond to heights below the smoke point, bold lines correspond to the smoke point height*

As mentioned before, at the same flame height the fuels can be in different sooting stages, and also have different fuel flow rates due to some differences in their vapour densities and flame structure. **Figure 6** shows a comparison of the PSD between the fuels at approx-

imately the same flow rate, toluene is not displayed because at this flow rate the flame has an opened undefined tip which could not be sampled due to rapid clogging of the probe. At this flow rate, heptane has a 5 mm bluish flame and the PSD consists of a large nucleation mode of particles below 10 nm. With the addition of toluene, H90T10 mixture corresponds to a 10 mm flame and the yellow luminosity of the flame is now visible, the PSD is bimodal with larger accumulation mode. For similar flame height H70H30 exhibits a bimodal PSD with a large dominant accumulation mode, and H50T50 which has 12 mm flame (above its smoke point) presents a strong accumulation mode of larger particles.

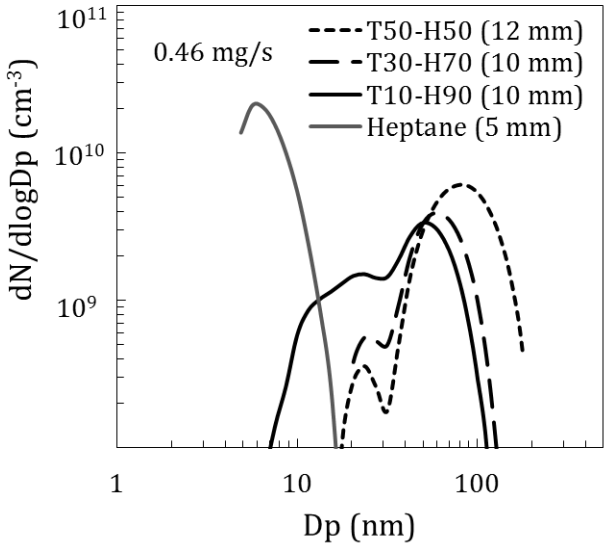

Figure 6: *PSDs at the flame tip of all the fuels at approximate 0.46 mg/s flow rate. Flame heights are given in parentheses.*

Figure 7 shows a comparison between PSDs of gasoline and H50T50 at the same flame heights. For the smallest flames of 3 and 4 mm height the PSDs are almost identical. As flame height increases the shape remains similar but gasoline forms less particles. Close to the smoke point, at 11 mm flame height, the PSDs are composed mainly of an accumulation mode or large agglomerates. At about the smoke point (approx. 12 mm) and above, the PSD of H50T50 are slightly shifted to larger sizes.

3.4 Soot morphology and primary particle size

Acknowledging the fact the that the particles formed in these flames are aggregates with non-spherical shape, we have taken TEM images to observe possible differences in their morphology. Particle morphology can give information on soot formation and oxidation inside the flame [11, 31, 32, 67].

The fuels selected for his analysis were: heptane, H50T50, gasoline and toluene. To compare flames at similar sooting stages we chose flames close to the smoke point (normalised flame height between 0.92 and 0.95). This corresponds to a 7, 11 and 11 mm flame for

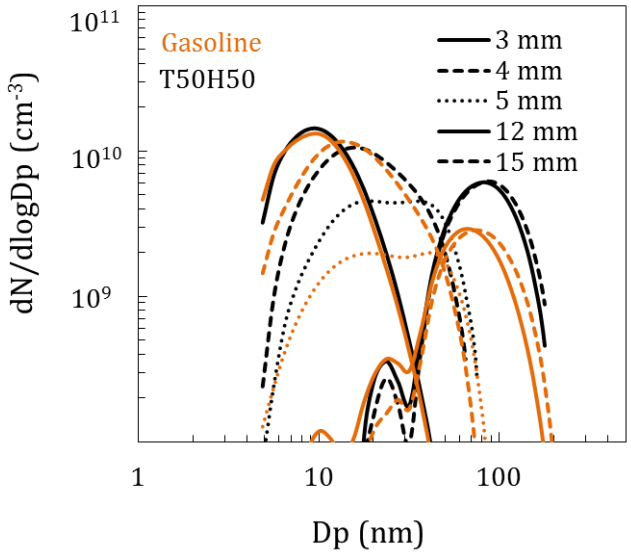

Figure 7: *PSDs of gasoline (orange) and 50/50 toluene-heptane mixture at the tip of different flame heights.*

toluene, H50T50 and gasoline respectively, for heptane a 40 mm flame was chosen. Heptane having such a large smoke point could not be sampled at the same sooting stage as the other fuels (equipment limitation plus the instability of very large flames did not allow it). Given the asymptotic behaviour of $\langle dp \rangle$ and N with normalised flame height observed for heptane, a flame height was chosen such that almost constant $\langle dp \rangle$ and N values were attained and flame stability allowed it.

The flames mentioned were sampled at the tip and inside the flame (at the centerline close to the tip). The measurements inside the flame were performed at 7, 7 and 30 mm height above de burner for H50T50, gasoline and heptane. Toluene was only sampled at the tip because such a small flame was extinguished when the sample probe was inserted inside of it.

Figure 8 presents representative TEM images of soot sampled at the tip (top row) and below the tip (bottom row) of flames of toluene, heptane, H50T50 and gasoline. It can be observed how the aggregate and primary particle size increases from heptane to H50T50 and gasoline, and the largest particles are formed by toluene. At the tip, soot produced from toluene appear to have much larger primary particle size and to be more dense and compact, with sphere-like primaries as well as bigger clumps without a clear shape. Soot produced from heptane appears as an agglomerate composed by clumps of very compact carbon as well as some recognisable smaller primary spheres. Instead, the aggregates produced from H50T50 and gasoline seem to be composed of nearly spherical primaries of similar sizes attached to each other in a less packed configuration.

Looking at the particles sampled below the flame tip, heptane shows mainly sphere-like particles of bigger size attached to each other, suggesting some kind of densification and shrinkage while moving to the tip. H50T50 and gasoline also show slightly larger primaries but a more dense configuration, which denotes possible oxidation of the outer edges as well as the attack of interior parts of the aggregate leaving 'holes' inside of it as

it travels to the flame tip.

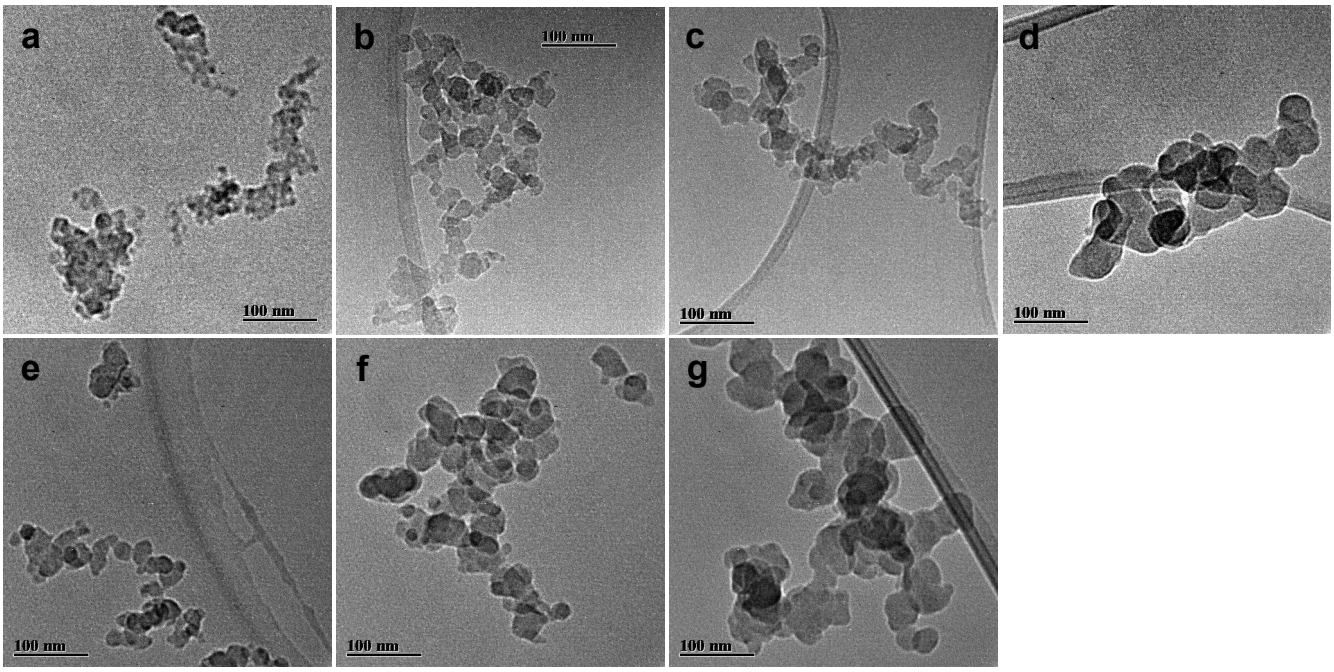

Figure 8: *TEM images of soot particles from different fuels at low resolution 40,000x. Top row: flame sampled at the tip; bottom row: flame sampled below the tip. a,e) Heptane; b,f) H50T50; c,g) Gasoline and d) Toluene.*

From the TEM images, the primary particle size (d_{PP}) of the aggregates was measured and fitted to a log-normal distribution and the results are presented in **Figure 9**. Solid lines represents the particles sampled at the tip of the flame and dashed lines represent the particles sampled below the tip of the flame. In both cases heptane exhibits the smallest d_{PP} followed by gasoline. H50T50 exhibits d_{PP} sizes larger than gasoline's and toluene presents the largest sizes. The size of primaries decreases from below the tip to the tip of the flame. The effect is more drastic for heptane than for the other fuels. This primary particle shrinking could be due to oxidation, which is closely related to flame temperature. Heptane exhibit temperatures in the range of 1650-1700 K at the sampling points, whereas H50T50 and gasoline present temperatures between 1300-1400 K, hence oxidation would be expected to be stronger for heptane.

4 Discussion

The addition of toluene (highly sooting fuel) to heptane (low sooting fuel) is known to have an increasing sooting effect. It has been shown before that the TSI of such blends increases linearly with toluene addition [22, 37, 65].

It is observed in the results of this investigation how the PSDs are shifted to larger aggregate diameters as toluene is added to heptane. For similar flow rates the effect of toluene addition is dramatic on the $\langle dp \rangle$ but not much on the number of particles as shown in **Fig-**

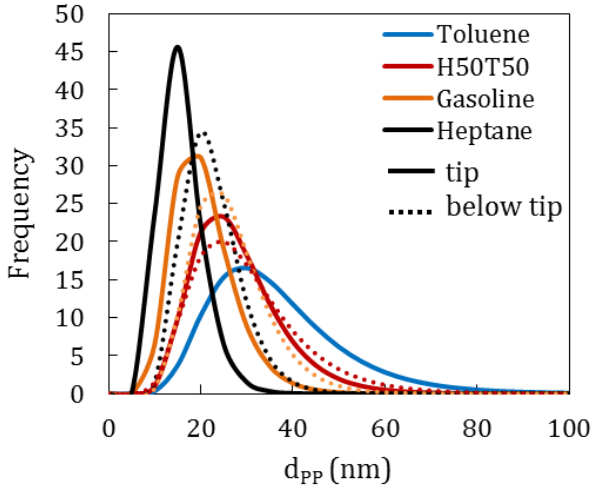

Figure 9: *Log-normal fits of primary particle size distribution of soot in the tip of an heptane flame of 40 mm, H50T50 flame of 11 mm, gasoline flame of 11mm and toluene flame of 7mm. Solid lines: flame sampled at the tip; dashed line: flame sampled below the tip.*

ures 4a, 4b. This may suggest that it is not the inception process but the particle growth that is affected by the increase in toluene concentration. It is noted that when comparing results at the same flow rates, specially at low values, the $\langle dp \rangle$ of some mixtures and pure toluene can be above $\sim$20 nm. These particles might not be newly incepted particles but single particles that have undergone surface growth or small agglomerates, indicating that such flames are in a relatively advanced sooting stage.

In **Figures 4c, 4d** flames at the same sooting stage (below and above the smoke point) can be compared. H70T30 and H90T10 exhibit values similar to heptane for both $\langle dp \rangle$ and N. It is clear that pure toluene and H50T50 mixture have larger particle numbers at the smaller normalised flame (even though they have lower flow rates hence residence time). This seems intuitive given that a greater abundance of toluene would result in intact aromatic radicals and species that enhances soot inception. And this enhanced particle production leads to more frequent collisions among particles, therefore more particles would appear to have diameters corresponding to aggregates.

Another interesting result is the different trends on the evolution of $\langle dp \rangle$ with flow rate. It was previously found in paraffin flames [5] that as flame height (equivalent to flow rate) was increased $\langle dp \rangle$ achieved a maximum value that remained almost constant with further flame height increases. The absence of growth of $\langle dp \rangle$ was attributed to a possible balance between particle growth and particle oxidation, particularly at larger flames where the peak temperature would be somewhere below the tip of the flame. Instead, toluene shows a continuous particle growth at the tip of the flame when the fuel flow rate is augmented. Results show that H90T10 mixture follows the same trend as paraffin fuels, although the $\langle dp \rangle$ are larger than those of heptane. H70T30 also behaves similar to paraffins with similar $\langle dp \rangle$ values until the smoke point, after which $\langle dp \rangle$ grows again in the same way aromatics do. H50T50 has a $\langle dp \rangle$ evolution similar to toluene with a slight $\langle dp \rangle$ growth

deceleration close to the smoke point, as other aromatic fuels with larger smoke point than toluene [6].

Figure 10a shows the influence of toluene on the $\langle dp \rangle$ at the tip of the luminous flame, for different flow rates. It is clear that$\langle dp \rangle$ increases with increasing toluene fraction. Also as flow rate increases so does the amount of carbon going into the flame this could imply more particles and possibly large ones. At the lowest flow rates particles were not detected indicating some tolerance to toluene addition, which is reduced with increasing flow rates. Similar results were found by *Choi et al* [9] in a counterflow diffusion flame using laser induced incandescence to measure soot volume fraction. The tolerance of toluene addition in the soot formation regime was about 30% v/v, while in the soot formation-oxidation regime it was around 20% v/v. At very low flow rates the tip of the flame is expected to be the same or very close to the stoichiometric diffusion flame, hence we expect it to behave as in a soot formation region. As the flow rate is increased the luminous flame is somehow larger than the diffusion flame [53], as indicated by temperature measurements (**Figure 3a**), hence we would expect it to behave as a soot formation-oxidation region. TEM results confirm the hypothesis of oxidation at the tip of these flames. The aggregate and primary particle shrink between a point close to and below the tip and the tip itself. This is also observed to be more dramatic in the case of heptane and is explained by the larger flame temperatures in its flames.

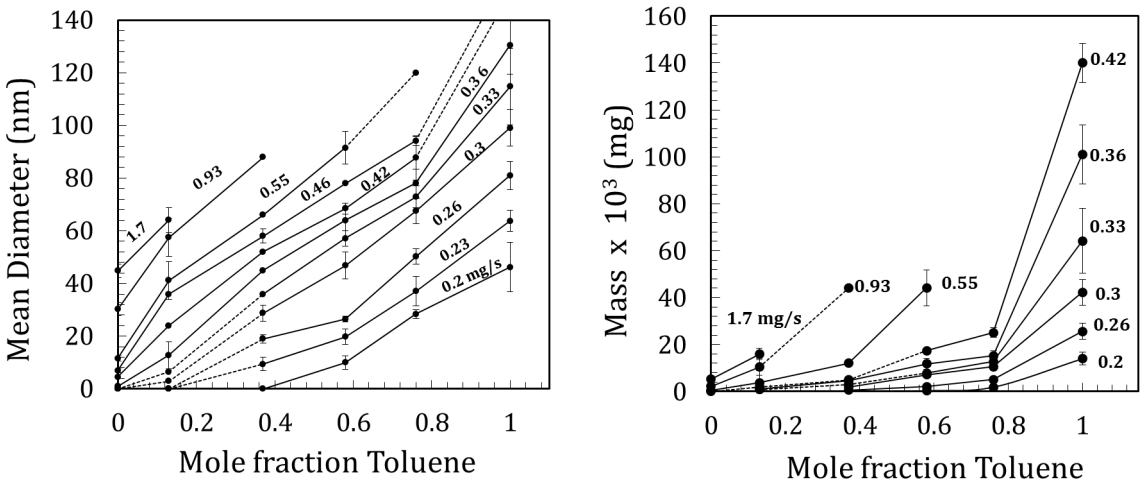

(a) *Mean particle diameter vs. percentage mol of toluene* **(b)** *Total soot mass vs. percentage mol of toluene*

Figure 10: *Mean particle size and mass of soot at the tip of the flame vs. toluene addition. Each line correspond to a different flow rate (flame height). Dashed lines are projections made according to the results in* ***Figure 4b****. Caption on lines correspond to fuel flow rate.*

To analyse the results obtained for the gasoline flame and be able to compare to the surrogate flames it is important to look at its composition and the temperature. For all flames heights the difference between the maximum temperature (most of the cases below the tip) of gasoline and H50T50 was between 50-80 K, having H50T50 higher maximum temperatures and also temperature profiles, this will favour fuel pyrolysis thus soot inception and growth. As shown by TEM images for one flame height, the primary particle size

of H50T50 was larger suggesting a larger particle surface growth. The images also show that oxidation does not play a dominant role for this fuels, the reason may be the overall low temperatures in these flames.

In terms of composition, although the toluene content of gasoline is high ($\sim$ 14% in mass) the majority of the aromatics present in this fuel are alkyl-substituted with larger and more substituents such as ethylbenzene, xylenes or trimethylbenzene. It is known that as the length of the side chain increases the sooting tendency of the aromatic fuel decreases (smoke point increases) [17, 28, 44]. Recently in a study of substituted aromatics [6] we found that the final $\langle dp \rangle$ at the flame tip was smaller for aromatic fuels substituted with larger chains.

In **Figure 11** we compare results of $\langle dp \rangle$ and N against normalised flame height for gasoline and H50T50 with previously reported results of n-butylbenzene (BB)[6]. It can be seen that for flames close to the smoke point and above the evolution of $\langle dp \rangle$ is very similar to that of BB. Eventhough H50T50 and the gasoline tested in this study had very similar temperature profiles and smoke point, the $\langle dp \rangle$ differ and this difference can be traced back to the highly complex composition of gasoline. The inclusion of larger alkylbenzenes in the formulation of surrogate fuels for a more realistic representation have been suggested by many researchers [10, 16, 19, 34], and is supported by the present results.

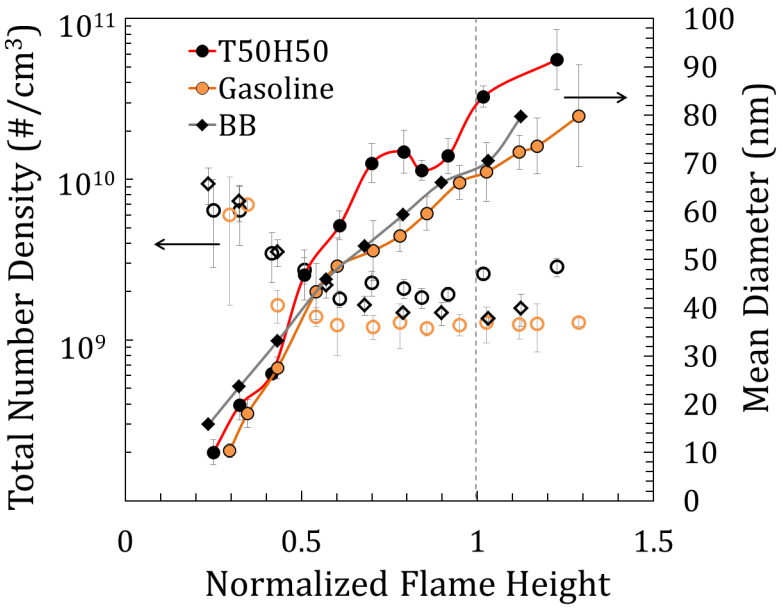

Figure 11: *Comparison of mean soot particle diameter and number of particles at the tip of the flames of Gasoline, H50T50 and Butylbenzene (BB) as a function flame height normalised by the smoke point.*

5 Conclusions

The temperature profiles, PSDs and morphology of soot particles formed in a wick-fed diffusion flame were measured using a fast insertion thermocouple/thermophoretic-sampling and probe sampling/differential mobility spectroscopy. The effect of aromatic composition in the sooting characteristics of fuels was studied in n-heptane/toluene mixtures, as well as in a commercial gasoline. Mean particle mobility size $\langle dp \rangle$ and aggregate number density N were evaluated at the tip of flames at different sooting stages. The following was observed:

- Two trends in the evolution of $\langle dp \rangle$ and N with flame height consistent with previous studies [5, 6]: 1) The paraffin-like trend where $\langle dp \rangle$ grows fast at the tip of small flame heights and achieve a maximum value that is sustained for larger flame heights and 2) the aromatic trend where $\langle dp \rangle$ grows continuously as flame height is increased, with as deceleration around the smoke point. As toluene is added to heptane the evolution of the PSD changes gradually from paraffin-like to aromatic. H90T10 mixture follows the same trend as paraffin fuels [5] with $\langle dp \rangle$ larger than those of heptane. H70T30 exhibits a transition between the two mentioned trends, below the smoke point $\langle dp \rangle$ values similar to paraffins, above the smoke point $\langle dp \rangle$ grows again in the same way aromatics do [6]. H50T50 has a $\langle dp \rangle$ evolution similar to toluene with a slight $\langle dp \rangle$ growth deceleration close to the smoke point, as other aromatic fuels with larger smoke point than toluene [6].

- The addition of toluene to heptane shifts the PSD and primary particle to larger diameters. The large particle mobility sizes ($\sim$20 nm) found at low flow rates for toluene and H50T50 indicate their relatively advanced sooting stage. A tolerance to toluene addition at the lowest flow rates was found, where particles were not detected. Increasing the flow rate increases $\langle dp \rangle$ due to the larger amount of carbon going into the flame.

- The studied gasoline has a smoke point and temperature profile close to those of heptane/toluene mixture with similar aromatic content (H50T50). The $\langle dp \rangle$ of gasoline follows an aromatic-like trend, but the values of $\langle dp \rangle$ and primary particle size are smaller than those of H50T50. This can be traced back to gasoline composition in which about 30% of the fuel are aromatics with more and larger substitutions than toluene. This type of aromatics have been shown to produce soot particles with smaller diameters [6]. It is important to consider other alkylated aromatics in the formulation of surrogate fuels to match the sooting characteristics of the real fuel.

6 Acknowledgments

M.B acknowledges financial support provided by the Administrative Department of Science, Technology and Innovation of Colombia. This project is funded by the National Research Foundation (NRF), Prime Minister's Office, Singapore under its Campus for Research Excellence and Technological Enterprise (CREATE) programme.

References

[1] M. Alfe, B. Apicella, R. Barbella, J.-N. Rouzaud, A. Tregrossi, and A. Ciajolo. Structure-property relationship in nanostructures of young and mature soot in premixed flames. *Proceedings of the Combustion Institute*, 32(1):697 – 704, 2009. ISSN 1540-7489. doi:10.1016/j.proci.2008.06.193.

[2] J. Appel, H. Bockhorn, and M. Frenklach. Kinetic modeling of soot formation with detailed chemistry and physics: laminar premixed flames of C2 hydrocarbons. *Combustion and Flame*, 121(1-2):122 – 136, 2000. ISSN 0010-2180. doi:10.1016/S0010-2180(99)00135-2.

[3] ASTM. Standard test method for smoke point of kerosine and aviation turbine fuel. *ASTM Standard D1322-08*, 1997.

[4] M. M. Aye, J. Beeckmann, A. Vanegas, N. Peters, and H. Pitsch. Experimental investigation of diesel and surrogate fuels: spray and ignition behaviour. *SAE technical paper*, (2011-01-1921), 2011. doi:10.4271/2011-01-1921.

[5] M. L. Botero, S. Mosbach, and M. Kraft. Sooting tendency of paraffin components of diesel and gasoline in diffusion flames. *Fuel*, 126:8 – 15, 2014. ISSN 0016-2361. doi:10.1016/j.fuel.2014.02.005.

[6] M. L. Botero, S. Mosbach, J. Akroyd, and M. Kraft. Sooting tendency of surrogates for the aromatic fractions of diesel and gasoline in a wick-fed diffusion flame. *Fuel*, 153:31 – 39, 2015. ISSN 0016-2361. doi:10.1016/j.fuel.2015.02.108.

[7] H. F. Calcote and D. M. Manos. Effect of molecular structure on incipient soot formation. *Combustion and Flame*, 49(1-3):289–304, 1983. doi:10.1016/0010-2180(83)90172-4.

[8] D. Chen, Z. Zainuddin, E. Yapp, J. Akroyd, S. Mosbach, and M. Kraft. A fully coupled simulation of PAH and soot growth with a population balance model. *Proceedings of the Combustion Institute*, 34(1):1827 – 1835, 2013. ISSN 1540-7489. doi:10.1016/j.proci.2012.06.089.

[9] B. Choi, S. Choi, and S. Chung. Soot formation characteristics of gasoline surrogate fuels in counterflow diffusion flames. *Proceedings of the Combustion Institute*, 33 (1):609 – 616, 2011. ISSN 1540-7489. doi:10.1016/j.proci.2010.06.067.

[10] M. Colket, T. Edwards, S. Williams, N. Cernansky, D. L. Miller, F. Egolfopoulos, P. Linstedt, R. Seshadri, F. L. Dryer, C. K. Law, D. G. Friend, D. Lenhert, H. Pitsch, A. Sarofim, M. Smooke, and W. Tsang. Development of an experimental database and kinetic models for surrogate jet fuels. *45th AIAA Aerospace Sciences Meeting and Exhibit Proceedings*, pages 1–21, 2007.

[11] M. M. Constatine and A. D. Richard. Comparison of soot growth and oxidation in smoking and non-smoking ethylene diffusion flames. *Combustion Science and Technology*, 66(1-3):1–16, 1989. doi:10.1080/00102208908947136.

[12] V. A. Cundy, J. S. Morse, and D. W. Senser. Constant-tension thermocouple rake suitable for use in flame mode combustion studies. *Review of Scientific Instruments*, 57(6):1209–1210, 1986. doi:10.1063/1.1138631.

[13] A. Diez, R. J. Crookes, and T. Løvås. Experimental studies of autoignition and soot formation of diesel surrogate fuels. *Proceedings of the Institution of Mechanical Engineers, Part D: Journal of Automobile Engineering*, 227(5):656 – 664, 2013. doi:10.1177/0954407012458402.

[14] R. A. Dobbins and C. M. Megaridis. Morphology of flame-generated soot as determined by thermophoretic sampling. *Langmuir*, 3(2):254–259, 1987. doi:10.1021/la00074a019.

[15] S. Dooley, S. H. Won, M. Chaos, J. Heyne, Y. Ju, F. L. Dryer, K. Kumar, C.-J. Sung, H. Wang, M. A. Oehlschlaeger, R. J. Santoro, and T. A. Litzinger. A jet fuel surrogate formulated by real fuel properties. *Combustion and Flame*, 157(12): 2333–2339, 2010. ISSN 0010-2180. doi:10.1016/j.combustflame.2010.07.001.

[16] S. Dooley, S. H. Won, J. Heyne, T. I. Farouk, Y. Ju, F. L. Dryer, K. Kumar, X. Hui, C.-J. Sung, H. Wang, M. A. Oehlschlaeger, V. Iyer, S. Iyer, T. A. Litzinger, R. J. Santoro, T. Malewicki, and K. Brezinsky. The experimental evaluation of a methodology for surrogate fuel formulation to emulate gas phase combustion kinetic phenomena. *Combustion and Flame*, 159(4):1444–1466, 2012. ISSN 0010-2180. doi:10.1016/j.combustflame.2011.11.002.

[17] F. Douce, N. Djebaoli-Chaumeix, C.-E. Paillard, C. Clinard, and J.-N. Rouzaud. Soot formation from heavy hydrocarbons behind reflected shock waves. *Proceedings of the Combustion Institute*, 28(2):2523 – 2529, 2000. ISSN 1540-7489. doi:10.1016/S0082-0784(00)80668-2.

[18] J. Etheridge, S. Mosbach, M. Kraft, H. Wu, and N. Collings. Modelling soot formation in a DISI engine. *Proceedings of the Combustion Institute*, 33(2):3159 – 3167, 2011. ISSN 1540-7489. doi:10.1016/j.proci.2010.07.039.

[19] J. T. Farrell, N. Cernansky, F. Dryer, C. K. Law, D. G. Friend, C. Hergart, R. M. McDavid, A. K. Patel, C. J. Mueller, and H. Pitsch. Development of an experimental database and chemical kinetic models for surrogate diesel fuels. *SAE technical paper*, 2007-01-0201, 2007. doi:10.4271/2007-01-0201.

[20] M. Frenklach. Reaction mechanism of soot formation in flames. *Physical Chemistry Chemical Physics*, 4:2028–2037, 2002. doi:10.1039/B110045A.

[21] M. Frenklach and H. Wang. *Soot Formation in Combustion - Mechanisms and Models*. Springer-Verlag, 1994.

[22] R. Gill and D. Olson. Estimation of soot thresholds for fuel mixtures. *Combustion Science and Technology*, 40(5):307–315, 1984.

[23] I. Glassman. Soot formation in combustion processes. *Symposium (International) on Combustion*, 22(1):295 – 311, 1989. ISSN 0082-0784. doi:10.1016/S0082-0784(89)80036-0.

[24] I. Glassman and R. A. Yetter. *Combustion*. Elsevier Inc., San Diego, California, USA, fourth edition, 2008. ISBN 9780120885732.

[25] A. Gomez, G. Sidebotham, and I. Glassman. Sooting behavior in temperature-controlled laminar diffusion flames. *Combustion and Flame*, 58(1):45–57, 1984. ISSN 0010-2180. doi:10.1016/0010-2180(84)90077-4.

[26] M. Hartmann, I. Gushterova, M. Fikri, C. Schulz, R. Schiel, and U. Maas. Auto-ignition of toluene-doped n-heptane and iso-octane/air mixtures: High-pressure shock-tube experiments and kinetics modeling. *Combustion and Flame*, 158(1): 172 – 178, 2011. ISSN 0010-2180. doi:10.1016/j.combustflame.2010.08.005.

[27] J. Hernandez, J. Sanz-Argent, J. Benajes, and S. Molina. Selection of a diesel fuel surrogate for the prediction of auto-ignition under HCCI engine conditions. *Fuel*, 87(6):655 – 665, 2008. ISSN 0016-2361. doi:10.1016/j.fuel.2007.05.019.

[28] R. A. Hunt. Relation of smoke point to molecular structure. *Industrial and Engineering Chemistry*, 45(3):602–606, 1953.

[29] S. Kook and L. M. Pickett. Soot volume fraction and morphology of conventional and surrogate jet fuel sprays at 1000-K and 6.7-MPa ambient conditions. *Proceedings of the Combustion Institute*, 33(2):2911 – 2918, 2011. ISSN 1540-7489. doi:10.1016/j.proci.2010.05.073.

[30] S. Kook and L. M. Pickett. Soot volume fraction and morphology of conventional fischer-tropsch, coal-derived, and surrogate fuel at diesel conditions. *SAE technical paper*, (2012-01-0678), 2012. doi:10.4271/2012-01-0678.

[31] U. Koylu, G. Faeth, T. Farias, and M. Carvalho. Fractal and projected structure properties of soot aggregates. *Combustion and Flame*, 100(4):621 – 633, 1995. ISSN 0010-2180. doi:10.1016/0010-2180(94)00147-K.

[32] T. Lu, C. S. Cheung, and Z. Huang. Size-resolved volatility, morphology, nanostructure, and oxidation characteristics of diesel particulate. *Energy & Fuels*, 26(10): 6168–6176, 2012. doi:10.1021/ef3010527.

[33] J. Luo, M. Yao, H. Liu, and B. Yang. Experimental and numerical study on suitable diesel fuel surrogates in low temperature combustion conditions. *Fuel*, 97(0):621 – 629, 2012. ISSN 0016-2361. doi:10.1016/j.fuel.2012.02.057.

[34] O. Mathieu, N. Djebaili-Chaumeix, C.-E. Paillard, and F. Douce. Experimental study of soot formation from a diesel fuel surrogate in a shock tube. *Combustion and Flame*, 156(8):1576 – 1586, 2009. ISSN 0010-2180. doi:10.1016/j.combustflame.2009.05.002.

[35] C. S. McEnally, U. O. Koylu, L. D. Pfefferle, and D. E. Rosner. Soot volume fraction and temperature measurements in laminar nonpremixed flames using thermocouples. *Combustion and Flame*, 109(4):701 – 720, 1997. ISSN 0010-2180. doi:10.1016/S0010-2180(97)00054-0.

[36] C. S. McEnally, L. D. Pfefferle, B. Atakan, and K. Kohse-Hoinghaus. Studies of aromatic hydrocarbon formation mechanisms in flames: Progress towards closing the fuel gap. *Progress in Energy and Combustion Science*, 32(3):247–294, 2006. ISSN 0360-1285. doi:10.1016/j.pecs.2005.11.003.

[37] A. Mensch, R. J. Santoro, T. A. Litzinger, and S.-Y. Lee. Sooting characteristics of surrogates for jet fuels. *Combustion and Flame*, 157(6):1097–1105, 2010. ISSN 0010-2180. doi:10.1016/j.combustflame.2010.02.008.

[38] J. H. Miller. Aromatic excimers: evidence for polynuclear aromatic hydrocarbon condensation in flames. *Proceedings of the Combustion Institute*, 30(1):1381 – 1388, 2005. ISSN 1540-7489. doi:10.1016/j.proci.2004.08.192.

[39] J. H. Miller, K. C. Smyth, and W. G. Mallard. Calculations of the dimerization of aromatic hydrocarbons: Implications for soot formation. *Symposium (International) on Combustion*, 20(1):1139 – 1147, 1985. ISSN 0082-0784. doi:10.1016/S0082-0784(85)80604-4. Twentieth Symposium (International) on Combustion.

[40] J. H. Miller, J. D. Herdman, C. D. Green, and E. M. Webster. Experimental and computational determinations of optical band gaps for PAH and soot in a N_2-diluted, ethylene/air non-premixed flame. *Proceedings of the Combustion Institute*, 34(2): 3669 – 3675, 2013. ISSN 1540-7489. doi:10.1016/j.proci.2012.05.054.

[41] N. Morgan, M. Kraft, M. Balthasar, D. Wong, M. Frenklach, and P. Mitchell. Numerical simulations of soot aggregation in premixed laminar flames. *Proceedings of the Combustion Institute*, 31(1):693 – 700, 2007. ISSN 1540-7489. doi:10.1016/j.proci.2006.08.021.

[42] N. Morgan, A. Smallbone, A. Bhave, M. Kraft, R. Cracknell, and G. Kalghatgi. Mapping surrogate gasoline compositions into RON/MON space. *Combustion and Flame*, 157(6):1122 – 1131, 2010. ISSN 0010-2180. doi:10.1016/j.combustflame.2010.02.003.

[43] S. Mosbach, M. S. Celnik, A. Raj, M. Kraft, H. R. Zhang, S. Kubo, and K.-O. Kim. Towards a detailed soot model for internal combustion engines. *Combustion and Flame*, 156(6):1156 – 1165, 2009. ISSN 0010-2180. doi:10.1016/j.combustflame.2009.01.003.

[44] A. Mouis, A. Menon, V. Katta, T. Litzinger, M. Linevsky, R. Santoro, S. Zeppieri, M. Colket, and W. Roquemore. Effects of m-xylene on aromatics and soot in laminar, N_2-diluted ethylene co-flow diffusion flames from 1 to 5 atm. *Combustion and Flame*, 159(10):3168 – 3178, 2012. ISSN 0010-2180. doi:10.1016/j.combustflame.2012.03.014.

[45] D. Olson, J. Pickens, and R. Gill. The effects of molecular structure on soot formation II. diffusion flames. *Combustion and Flame*, 62(1):43–60, 1985.

[46] R. I. Patterson and M. Kraft. Models for the aggregate structure of soot particles. *Combustion and Flame*, 151(1 2):160 – 172, 2007. ISSN 0010-2180. doi:10.1016/j.combustflame.2007.04.012.

[47] W. Pitz, N. Cernansky, F. Dryer, F. Egolfopoulos, J. T. Farrell, D. G. Friend, and H. Pitsch. Development of an experimental database and chemical kinetic models for surrogate gasoline fuels. *SAE technical paper*, 2007-01-0175, 2007. doi:10.4271/2007-01-0175.

[48] A. Raj, M. Celnik, R. Shirley, M. Sander, R. Patterson, R. West, and M. Kraft. A statistical approach to develop a detailed soot growth model using PAH characteristics. *Combustion and Flame*, 156(4):896 – 913, 2009. ISSN 0010-2180. doi:10.1016/j.combustflame.2009.01.005.

[49] A. Raj, M. Sander, V. Janardhanan, and M. Kraft. A study on the coagulation of polycyclic aromatic hydrocarbon clusters to determine their collision efficiency. *Combustion and Flame*, 157(3):523 – 534, 2010. ISSN 0010-2180. doi:10.1016/j.combustflame.2009.10.003.

[50] M. Sander, R. I. Patterson, A. Braumann, A. Raj, and M. Kraft. Developing the PAH-PP soot particle model using process informatics and uncertainty propagation. *Proceedings of the Combustion Institute*, 33(1):675 – 683, 2011. ISSN 1540-7489. doi:10.1016/j.proci.2010.06.156.

[51] R. Santoro, H. Semerjian, and R. Dobbins. Soot particle measurements in diffusion flames. *Combustion and Flame*, 51:203–218, 1983. ISSN 0010-2180. doi:10.1016/0010-2180(83)90099-8.

[52] R. Schalla and G. McDonald. Variation in smoking tendency among hydrocarbons of low molecular weight. *Industrial and Chemical Chemistry*, 45(7):1497–1500, 1953.

[53] K. Schug, Y. Manheimer-Timnat, P. Yaccarino, and I. Glassman. Sooting behavior of gaseous hydrocarbon diffusion flames and the influence of additives. *Combustion Science and Technology*, 22:235–250, 1980.

[54] K. Siegmann, K. Sattler, and H. Siegmann. Clustering at high temperatures: carbon formation in combustion. *Journal of Electron Spectroscopy and Related Phenomena*, 126(1-3):191 – 202, 2002. ISSN 0368-2048. doi:10.1016/S0368-2048(02)00152-4.

[55] A. J. Smallbone, A. N. Bhave, N. Morgan, M. Kraft, R. Cracknell, and G. Kalghati. Simulating combustion of practical fuels and blends for modern engine applications using detailed chemical kinetics. *SAE technical paper*, 2010-01-0572, 2010. doi:10.4271/2010-01-0572.

[56] A. J. Smallbone, A. R. Coble, A. N. Bhave, S. Mosbach, M. Kraft, N. Morgan, and G. Kalghati. Simulating PM emissions and combustion stability in gasoline/diesel fuelled engines. *SAE technical paper*, 2011-01-1184, 2011. doi:10.4271/2011-01-1184.

[57] K. C. Smyth, J. Miller, R. C. Dorfman, W. Mallard, and R. J. Santoro. Soot inception in a methane/air diffusion flame as characterized by detailed species profiles. *Combustion and Flame*, 62(2):157 – 181, 1985. ISSN 0010-2180. doi:10.1016/0010-2180(85)90143-9.

[58] C. M. Sorensen. The mobility of fractal aggregates: A review. *Aerosol Science and Technology*, 45(7):765–779, 2011. doi:10.1080/02786826.2011.560909.

[59] T. S. Totton, D. Chakrabarti, A. J. Misquitta, M. Sander, D. J. Wales, and M. Kraft. Modelling the internal structure of nascent soot particles. *Combustion and Flame*, 157(5):909 – 914, 2010. ISSN 0010-2180. doi:10.1016/j.combustflame.2009.11.013.

[60] M. Velasquez, F. Mondragon, and A. Santamaria. Chemical characterization of soot precursors and soot particles produced in hexane and diesel surrogates using an inverse diffusion flame burner. *Fuel*, 104:681 – 690, 2012. ISSN 0016-2361. doi:10.1016/j.fuel.2012.04.033.

[61] H. Wang. Formation of nascent soot and other condensed-phase materials in flames. *Proceedings of the Combustion Institute*, 33(1):41 – 67, 2011. ISSN 1540-7489. doi:10.1016/j.proci.2010.09.009.

[62] H. Wang and M. Frenklach. A detailed kinetic modeling study of aromatics formation in laminar premixed acetylene and ethylene flames. *Combustion and Flame*, 110 (1 - 2):173 – 221, 1997. ISSN 0010-2180. doi:10.1016/S0010-2180(97)00068-0.

[63] H. Wang, X. You, A. V. Joshi, S. G. Davis, A. Laskin, F. Egolfopoulos, and C. K. Law. USC mech version II. high-temperature combustion reaction model of H2/CO/C1-C4 compounds, May 2007.

[64] H. Wang, Q. Jiao, M. Yao, B. Yang, L. Qiu, and R. D. Reitz. Development of an n-heptane/toluene/polyaromatic hydrocarbon mechanism and its application for combustion and soot prediction. *International Journal of Engine Research*, 14(5): 434 – 451, 2013. doi:10.1177/1468087412471056.

[65] R. J. Watson, M. L. Botero, C. J. Ness, N. M. Morgan, and M. Kraft. An improved methodology for determining threshold sooting indices from smoke point lamps. *Fuel*, 111:120 – 130, 2013. ISSN 0016-2361. doi:10.1016/j.fuel.2013.04.024.

[66] D. Witkowski, K. Kondo, G. Vishwanathan, and D. Rothamer. Evaluation of the sooting properties of real fuels and their commonly used surrogates in a laminar co-flow diffusion flame. *Combustion and Flame*, 160(6):1129 – 1141, 2013. ISSN 0010-2180. doi:10.1016/j.combustflame.2013.01.027.

[67] J. Zhu, K. O. Lee, A. Yozgatligil, and M. Y. Choi. Effects of engine operating conditions on morphology, microstructure, and fractal geometry of light-duty diesel engine particulates. *Proceedings of the Combustion Institute*, 30(2):2781 – 2789, 2005. ISSN 1540-7489. doi:10.1016/j.proci.2004.08.232.